Optics Communications 285 (2012) 5029–5036

Contents lists available at SciVerse ScienceDirect

Optics Communications

journal homepage: www.elsevier.com/locate/optcom

Optical surface profile measurement using phase retrieval by tuning the illumination wavelength

Peng Bao*, Giancarlo Pedrini, Wolfgang Osten

Institut für Technische Optik, Universität Stuttgart, Pfaffenwaldring 9, 70569 Stuttgart, Germany

ARTICLE INFO

Article history:
Received 13 June 2012
Received in revised form
3 August 2012
Accepted 4 August 2012
Available online 23 August 2012

Keywords:
Metrology
Surface measurements
Figure
Phase retrieval
Image reconstruction techniques
Holography

ABSTRACT

In this paper, we present a method for measuring the surface profile of an object by using diffraction intensity patterns recorded at different illumination wavelengths. The main advantages of this technique are: simple optical set-up, high immunity to noise and environmental disturbance, since no reference beam (like in holography) or additional moving parts are needed. Two iterative calculations are synchronously performed using two sequences of diffraction intensity patterns, producing fast convergence to the expected result. The effects of different parameters on the accuracy and efficiency of the method are investigated. Simulation and experimental results are presented.

1. Introduction

Optical full field methods are well suited for the measurement of object shapes [1,2] and several techniques, such as grating or fringe projection [3,4], low coherence interferometry [5,6] and wavelength-scanning interferometry [7], have been proposed for determining the profile of large (some square meters) and microscopic structures. Digital holography, which became feasible along with the development of electronic recording devices (CCDs and CMOS), has been widely applied for the investigation of technical objects and biological samples [8,9] and some setups based on this technique have been used for measuring the surface profile and for quality control. Phase-shifting digital holography allows high accuracy in the reconstruction of three-dimensional objects [10,11]. By using a coherent mask produced by a spatial light modulator, the shapes of test objects can be remotely compared with a master object by the holographic technique [12,13]. However, conventional digital holography requires a reference beam and this can be a limitation. In particular when the source has low temporal coherence (e.g. excimer laser), a tedious and sometimes cumbersome process of optimizing the path length between object and reference beams is necessary. Beside the coherence requirements, attention has to be paid to the robustness of the set-up with respect to external influences such as vibrations and air turbulences.

A lot of effort has been directed to make interferometrical methods insensitive to environmental influences and investigations have been made with the purpose to reconstruct amplitude and phase without using reference beams and thus avoiding the disadvantages described above [14–17]. In this case, a pixelated detector is used to record different intensities of diffraction patterns while some experimental parameters are changed; the phase distribution is then recovered by iterative processing the recorded intensities. To acquire enough intensities of diffraction patterns, some techniques were used, such as moving an aperture inside the wavefront to record a sequence of intensities from different parts of the object [18], displacing the recording camera to record intensities at different planes [19,20] and moving a phase mask to record different modulated intensities [21]. These arrangements require the use of external mechanical moving devices (e.g. for displacing the aperture, the phase mask or the camera) and are thus sensitive to the environmental disturbance. A deformable mirror can be used to avoid the requirements of moving devices [22]. By using a designed periphery, the transmission test object can be reconstructed from one intensity measurement [23]. The phase retrieval techniques using multiple illumination wavelengths has an extended measurement range and does not require external moving devices [24,25].

Here we present a method where two iteration calculations are synchronously performed using two sequences of diffraction intensity patterns recorded at different wavelengths. This technique has fast convergence speed and high accuracy.

* Corresponding author.
E-mail address: itobaope@ito.uni-stuttgart.de (P. Bao).

0030-4018/$ - see front matter © 2012 Elsevier B.V. All rights reserved.
http://dx.doi.org/10.1016/j.optcom.2012.08.018

2. Set-up and algorithms

2.1. Experimental set-up

Fig. 1 shows the set-up used for the investigations. The beam emitted by a tunable laser is at first coupled into a fiber. The light at the fiber output is collimated (plane wave) and illuminates the object. An aperture in front of test sample limits the measurement area and a camera, located at the distance Z from the object, records a set of diffraction intensities obtained by changing the illumination wavelength. Fig. 1 shows an in-line setup for probing transmitting sample. For the investigation of reflecting objects, a beam splitter should be introduced between the collimator and the test object, and the camera should be placed after the beam splitter.

Fig. 2 shows the relation between the surface profile and the optical phase of a test object. We assume transparent objects made of isotropic material. For the sake of simplicity we consider the one-dimensional case where the profile is described by a continuous function $\Delta h(s)$ (Fig. 2a), by sampling $\Delta h(s)$ at intervals Δs (Fig. 2b) we get an array $\Delta h(l\Delta s)$, which is used to approximate the profile of the test surface. l is an integer number and in the following treatment we will simply denote the profile at $l\Delta s$ by $\Delta h(x)$. When the object is illuminated by a plane wave having wavelength λ, the phase change due to the object is

$$\Delta\phi(x)=\frac{2\Delta\pi h(x)}{\lambda}(n_{obj}-n_{air}) \tag{1}$$

where, n_{obj} and n_{air} are the refractive index of the material from which the object is made and air, respectively. For reflecting objects, the relation between phase and object profile is

$$\Delta\phi(x)=-\frac{4\Delta\pi h(x)}{\lambda} \tag{2}$$

Here the illumination beam goes though the optical path twice and the highest position of the surface has the lowest phase delay. According to Eqs. (1–2), the phase distribution is proportional to the surface profile and inversely proportional to the illumination wavelength. Notice that in the cases of transparent objects the dispersion of the test material should be considered and compensated.

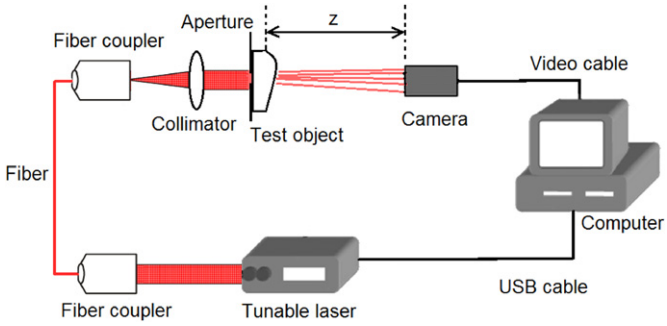

Fig. 1. Schematic of the measurement system.

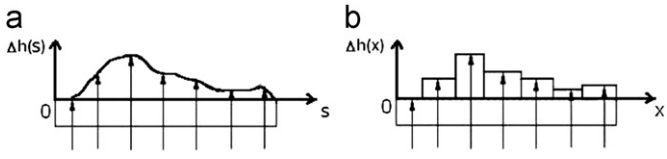

Fig. 2. Physical model of a transparent object (one dimensional): continuous curve (a) and discrete array (b).

2.2. Limitations of the phase retrieval method using single sequence intensity patterns (PRSS)

The PRSS methods can be used to get a wrapped phase and after application of an unwrapping procedure the object profile can be obtained [24,25]. However, the phase cannot be unwrapped until the iteration is completed. The relation between the wrapped phases ϕ_k and unwrapped phases ϕ_{unw_k} is

$$\phi_k(x',y')=\phi_{unw\_k}(x',y')+N(x',y')2\pi \quad N(x',y')=0,\pm1,\pm2\ldots \tag{3}$$

where the subscript k indicates the illumination wavelength λ_k. The process for retrieving the phase is shown in Fig. 3 [24,25]. The relation between the phases and the wavelengths is

$$\begin{aligned}\phi_{k+a}(x',y')&=\frac{\lambda_k}{\lambda_{k+a}}\phi_k(x',y')=\frac{\lambda_k}{\lambda_{k+a}}\phi_{unw\_k}(x',y')+\frac{\lambda_k}{\lambda_{k+a}}N(x',y')2\pi\\&=\frac{\lambda_k}{\lambda_{k+a}}\phi_{unw\_k}(x',y')+\left|\frac{\lambda_k}{\lambda_{k+a}}-1\right|N(x',y')2\pi+N(x',y')2\pi\end{aligned} \tag{4}$$

Here the indicator "a" is 1 or -1 and is used to keep the value of k valid: when $k+a>K$, the value of a is changed to -1; when $k+a<1$, the value of a is changed to 1.

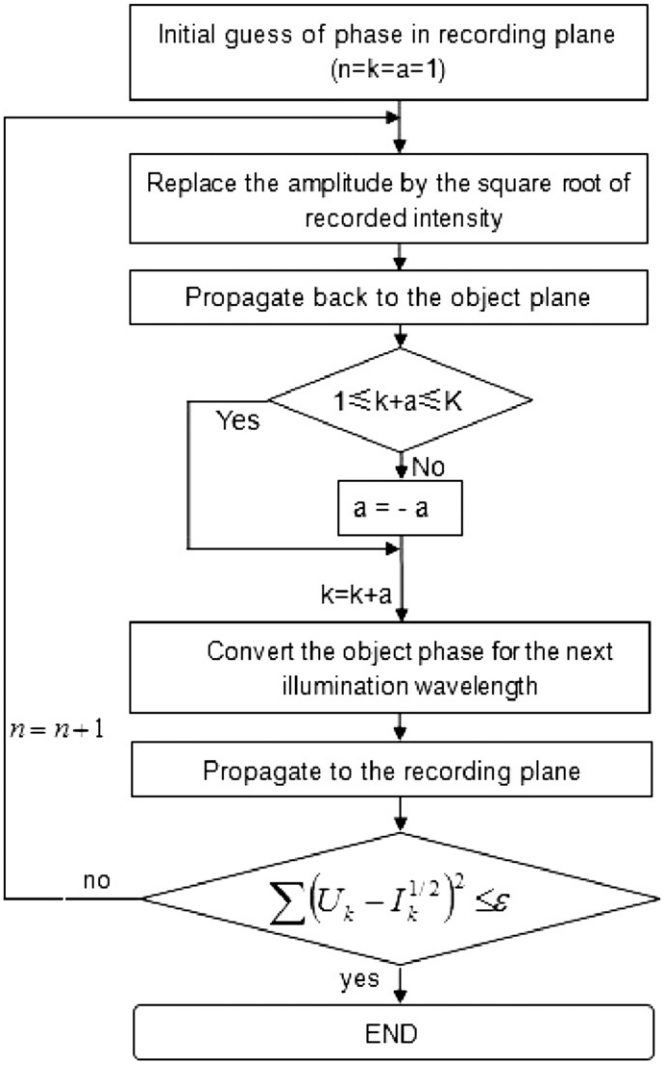

Fig. 3. Flowchart of the PRSS: n is the iteration number; k is the serial number of the used illumination wavelength; I_k is the recorded intensity; U_k is the calculated amplitude; a is the indicator; K is the total number of recorded intensities.

We define the factor: $\gamma = \left|\frac{\lambda_k}{\lambda_{k+a}} - 1\right|$. In the PRSS method, the terms $\gamma \cdot N(x',y')2\pi$ and $N(x',y')2\pi$ are neglected during the calculation, since the value of $N(x',y')$ is unknown. This may introduce errors whose magnitude depends on the height variation of the object surface and γ. Fig. 4 shows the influences of γ on the SNR (Signal to Noise Ratio) of the calculated phase. The SNR is defined as

$$SNR = 10\log_{10}\frac{\sum_{x,y}\left|\phi_{unw\_k}(x,y)\right|^2}{\sum_{x,y}\left|\phi_k(x,y)-\phi_{unw\_k}(x,y)\right|^2} \tag{5}$$

To proof the approach, a free-form surface object profile is used (Fig. 4a). Its refraction index is assumed to be 1.5, and the first illumination wavelength is set to 850 nm. The results show that the SNR decreases when γ and the profile height variation increase (Fig. 4b). The SNR is high when $\gamma = 0.001$, which means that the equivalent percent difference in wavelengths is only 0.1%, even when the object surface variation is larger than 50 μm. The SNR is only 20 dB when $\gamma = 0.2$ and the height variation of the object surface is 10 μm. The SNR reduction limits the PRSS, γ may be kept small but in this case many intensity patterns should be recorded. A discussion of the accuracy of the iterative phase retrieval methods is given in Ref. [26].

2.3. Phase retrieval using double sequences intensity patterns (PRDS)

In order to avoid the limitations described in section 2.2, a method using a double sequence has been developed. Fig. 5 shows the main procedure of PRDS. A set of intensities is recorded by using the set-up shown in Fig. 1, then the intensities are divided into two groups (I_t, recorded with λ_t, $t = 1,2,..T$; I_q, recorded with λ_q, $q = 1,2,..Q$). Note that the number of intensities in each group (T and Q) can be different and that the same pattern can be used twice. Two iterative calculations start simultaneously with two guessed phases (constant or random) at the recording plane and proceed as follows:

(1) Combine the calculated phases with the square roots of the recorded intensities (amplitudes) yielding two wavefronts

$$(a)\quad U_t(x,y) = \sqrt{I_t}\exp\left\{i\phi_q(x,y)\right\}$$
$$(b)\quad U_q(x,y) = \sqrt{I_q}\exp\left\{i\phi_q(x,y)\right\} \tag{6}$$

Note that two initial guessed phases are used in the first calculation.

(2) Propagate these two wavefronts back to the object plane.

(3) Calculate the object surface profile from the two phases.

$$h(x',y') = \frac{\Lambda}{c}\frac{\left|\phi_t(x',y')-\phi_q(x',y')\right|}{2\pi},\ \Lambda = \frac{\lambda_t\lambda_q}{\left|\lambda_t-\lambda_q\right|},\ \lambda_t \neq \lambda_q \tag{7}$$

where $h(x',y')$ is the surface height profile, $\phi_t(x',y')$ and $\phi_q(x',y')$ are the object phase calculated in each iterative calculations; $c = -2$ for reflecting and $c = n_{obj} - n_{air}$ for transmitting samples, respectively (see Eqs. 1 and 2), Λ is the synthetic wavelength.

(4) Combine the average of the object amplitudes ($A_t(x',y')$ and $A_q(x',y')$) and phases at different illumination wavelengths yielding two wavefronts at the object plane.

$$(a)\quad U_{t+a}(x',y') = \frac{A_t(x',y')+A_q(x',y')}{2}\exp\left\{2\pi i\frac{h(x',y')}{\lambda_{t+a}}\right\}$$
$$(b)\quad U_{q+b}(x',y') = \frac{A_t(x',y')+A_q(x',y')}{2}\exp\left\{2\pi i\frac{h(x',y')}{\lambda_{q+b}}\right\} \tag{8}$$

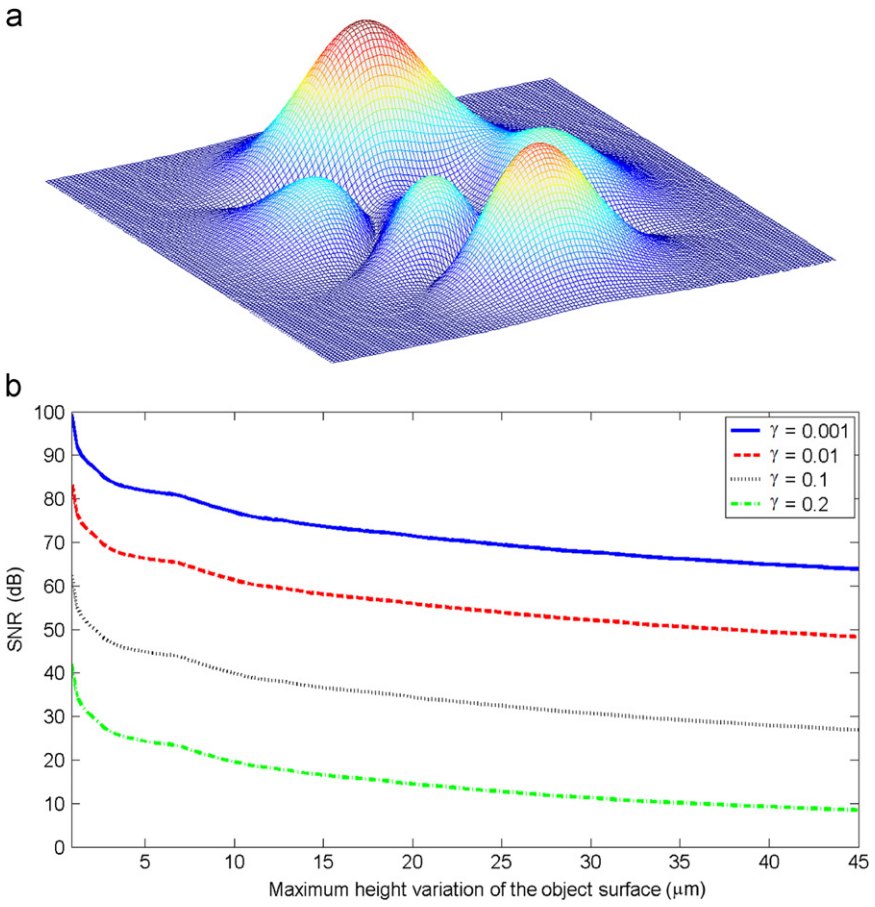

Fig. 4. Influences on the SNR: (a) object: a free-form surface; (b) the SNR curves versus the maximum height ($\Delta h_{\wedge}$) of the surface profile.

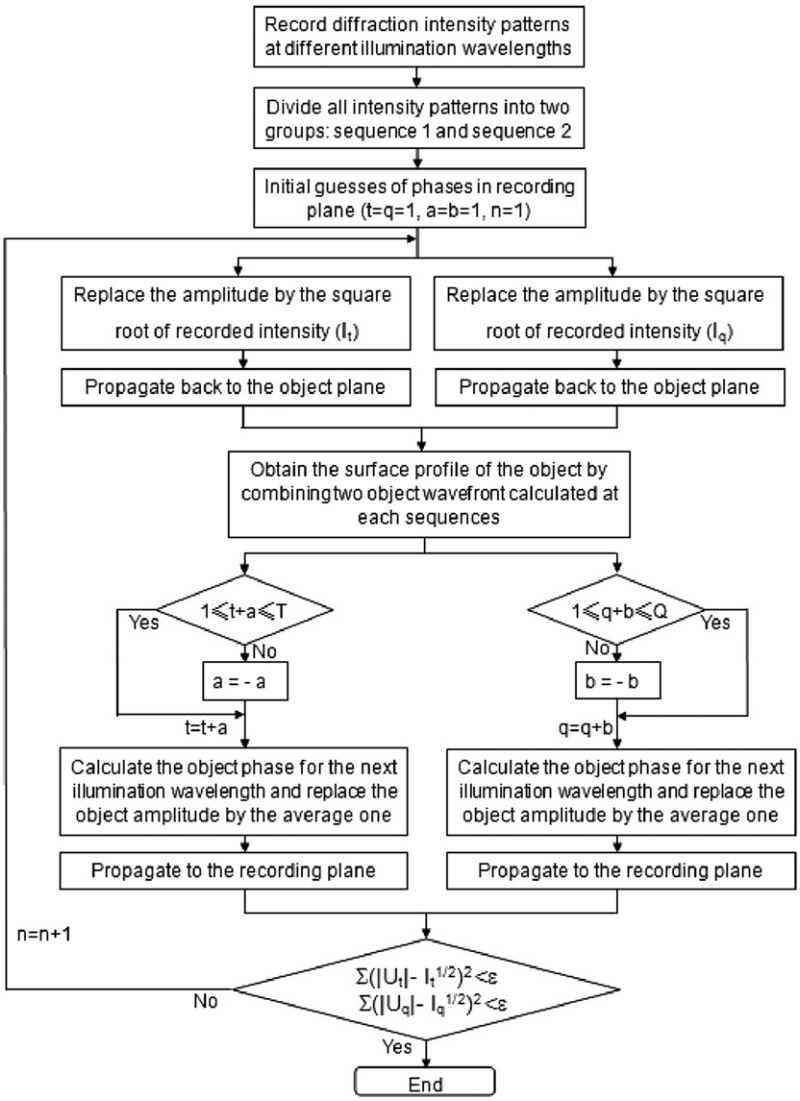

Fig. 5. Flowchart of the PRDS: n is the iteration number; t and q are the serial numbers of the illumination wavelengths; a and b are indicators; I_t and I_q are the recorded intensities; U_t and U_q are the calculated amplitudes; T and Q are the total number of recorded intensities in each groups.

The parameters a, b take the values 1 or -1 and are used to keep valid the values of t and q.

(5) Propagate these two wavefronts to the recording plane.
(6) Repeat the steps 1 to 5.

This procedure ends when both the differences between the calculated and recorded intensities are sufficiently small. For the beam propagation in steps 2 and 5, the angular spectrum or Fresnel algorithms can be used [27]. The two sequences of wavelengths should be arranged to ensure that the synthetic wavelength is larger than the maximum height variation of the object surface each time the step 3 is executed, otherwise the SNR may be reduced.

3. Results and discussions

3.1. Comparisons of convergence performances between PRDS and PRSS

Fig. 6 shows the pattern used for the simulations, the gray level indicates the height profile of a transmitting object having

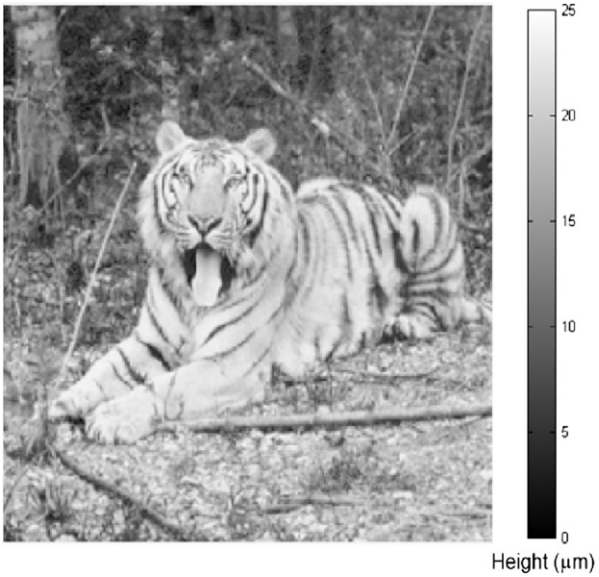

Fig. 6. Test object used for the simulations. The gray level indicates the height value (0–25 μm).

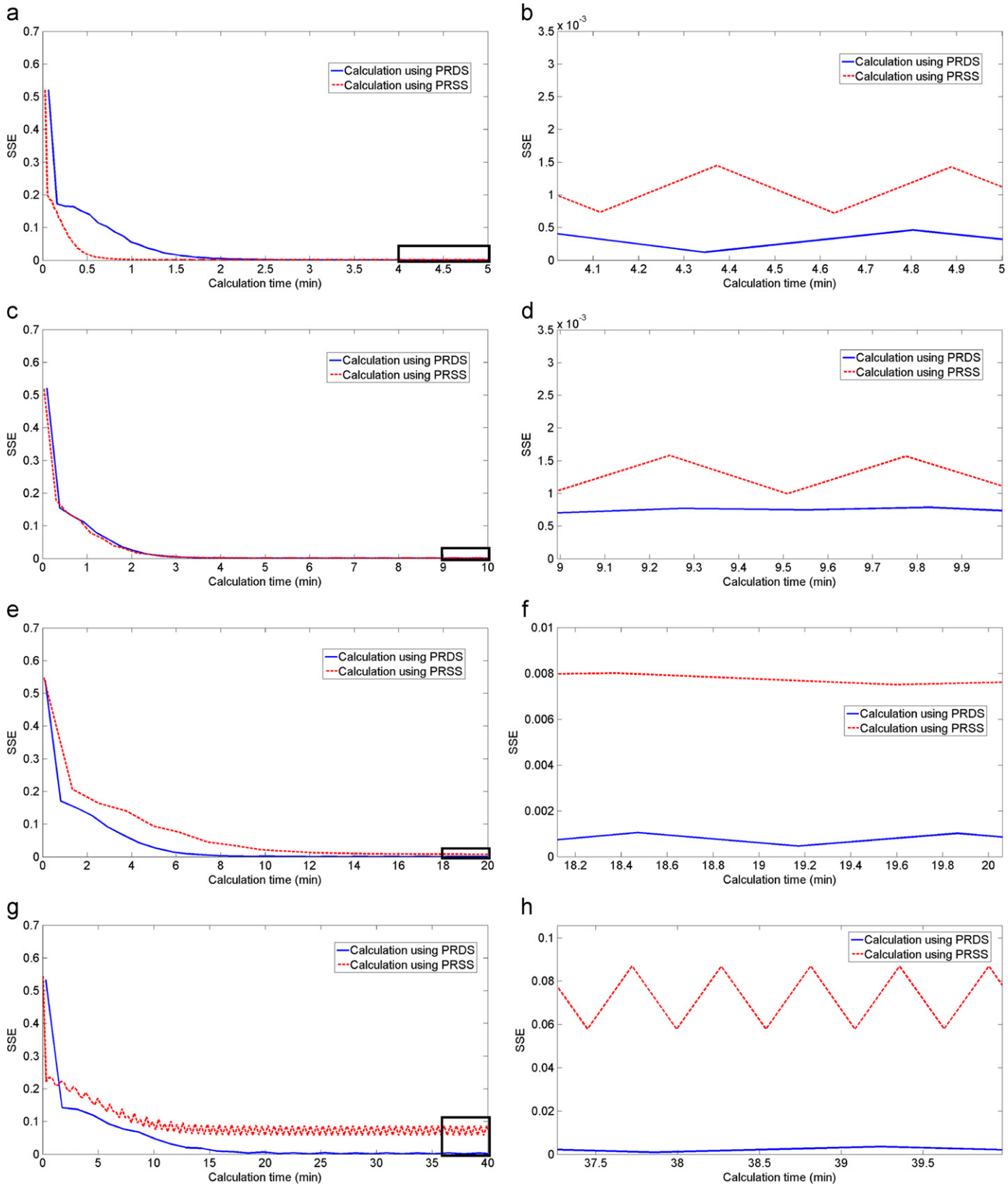

Fig. 7. Comparison between the PRDS and the PRSS methods. Convergence curves and their magnified parts when: $\Delta h_{\wedge}=2\ \mu m$(a) and (b); $\Delta h_{\wedge}=10\ \mu m$ (c) and (d); $\Delta h_{\wedge}=20\ \mu m$ (e) and (f); $\Delta h_{\wedge}=85\ \mu m$ (g) and (h).

refraction index 1.5. The test object is limited by a square aperture ($5\times5\ mm^2$). The distance between the object and the sensor is 30 mm, the sensor has 1000×1000 pixels, the pixel size is $6\times6\ \mu m^2$. Eleven diffraction patterns recorded at wavelengths from 750 nm to 850 nm with an interval of 10 nm were used for the comparison between PRSS and PRDS. For the PRSS we use

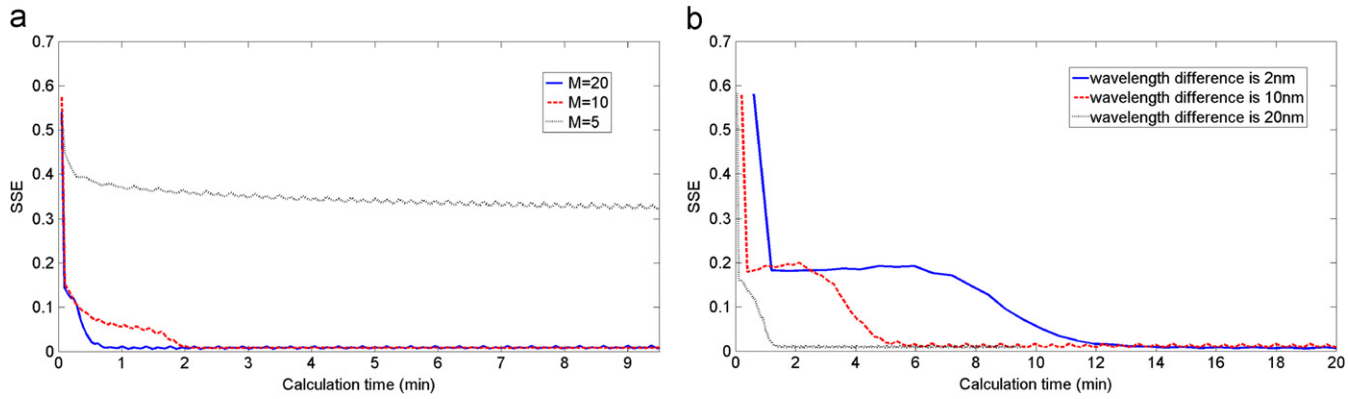

Fig. 8. Convergence performance: (a) different numbers of intensity patterns $M=5$, 10, and, 20; (b) different wavelength differences $|\lambda_t-\lambda_q|=2$ nm, 10 nm and 20 nm.

intensities recorded at the wavelength.

$$\lambda_n = 850\text{ nm}, 840\text{ nm}, 830\text{ nm}, \ldots 750\text{ nm} \quad n = 1, 2, 3, \ldots, 11 \tag{9}$$

For the PRDS method the diffraction patterns are divided into two sequences, each of them contains 10 diffraction patterns

$$\lambda_t = 850\text{ nm}, 840\text{ nm}, 830\text{ nm}, \ldots 760\text{ nm} \quad t = 1, 2, 3, \ldots, 10$$

$$\lambda_q = 840\text{ nm}, 830\text{ nm}, 820\text{ nm}, \ldots 750\text{ nm} \quad q = 1, 2, 3, \ldots, 10 \tag{10}$$

To quantify the accuracy and convergence of these two methods, the sum-squared error (SSE), defined as

$$SSE = \frac{\sum_{m,n}\left[|U(m,n)|-|\overline{U}(m,n)|\right]^2}{\sum_{m,n}|U(m,n)|^2} \tag{11}$$

is used, where $U(m,n)$ and $\overline{U}(m,n)$ represent the original and the recovered object wavefronts.

The convergence behavior of the PRDS and PRSS methods is different when the height variations of the object surface become larger. The maximum height ($\Delta h_{\wedge}$) determines the variation range of the object surface. When $\Delta h_{\wedge}=2$ μm, which corresponds to about 2.35π at 850 nm wavelength, the curve of PRSS converges faster (Fig. 7a); however, the final result obtained by using PRDS is better (Fig. 7b). When $\Delta h_{\wedge}=4$ μm, the convergence speed is almost the same (Fig. 7c), while the final result of PRDS is better (Fig. 7d). When $\Delta h_{\wedge}$ increases to 2.0 μm, the curve of the PRDS converge faster than PRSS (Fig. 7e), and the final SSE of PRDS is much lower than PRSS (Fig. 7f). When $\Delta h_{\wedge}=85$ μm, the curve of PRSS have a SSE level of 0.01, which means it does not converge (Fig. 7g). On the other hand, good result can be obtained using PRDS (Fig. 7g and h). The comparisons show that the PRDS is more suitable for measuring objects with large height variation surface. When the height variation of the object surface is not so large, PRDS and PRSS can be chosen in order to balance the calculation speed and the SSE.

3.2. Convergence performances of PRDS under different conditions

The object and the sensor described above have been used to evaluate the influences of some parameters. The wavelengths for the illumination were between 630 nm and 850 nm and $\Delta h_{\wedge}=25$ μm. According to Eq. (7), the synthetic wavelength Λ should satisfy the relation: $\Lambda \geq c\Delta h_{max}$. In this simulation we choose $c=0.5$ and thus $\Lambda > 12.5$ μm. Fig. 8(a) shows the performance of the PRDS method depending from the number of used illumination wavelengths. When the number of intensity patterns was reduced from 20 to 10, the convergence rate slowed by a factor 2.5, and the final SSE did not change. The reason is that the information provided by 10 patterns is enough to get convergence. However, the algorithm did not converge when only 5 patterns were used.

The results shown in Fig. 8(b) were obtained by using $M=21$ intensity patterns; a maximum illumination wavelength of 850 nm and $|\lambda_t-\lambda_q|=2$ nm, 10 nm and 20 nm. Thus the corresponding synthetic wavelength Λ in each iteration (see Eq. (7)) varies in the ranges: [210.6 μm–360.4 μm], [41.6 μm–71.4 μm] and [20.475 μm–35.275 μm], respectively. The convergence curves show that the convergence slows down when the synthetic wavelengths increase; while the converged SSE remains the same. The reason of these behaviors is that when a large synthetic wavelength is used, the calculation is sensitive to small changes of unwrapped phase at the beginning of the iteration process.

3.3. Experimental results

Experiments were performed in order to verify the method. The light source was a Titanium-Sapphire laser (Matisse-TR, produced by Sirah GmbH) with a wavelength tuning range between 750 nm and 850 nm. The coherence length is more than 30 m and the wavelength bandwidth narrower than 0.00002 nm. The camera was a PCO Imaging Pixelfly QE having 1392×1024 pixels of size 6.45×6.45 μm^2. Only 1024×1024 pixels were used to get efficient FFT calculation. The tunable laser and the camera were linked via USB and video cables to a computer which control the change of wavelength and the intensity recording. A computer with AMD 2.8 GHz processor and 8 GB memory was used for the evaluation.

The test object was a microlens array located at the distance 30 mm from the CCD sensor. The microlens array is made of silica, the dispersion of this material can be found in Ref. [28].Twenty-one wavelengths were used to get the results. Fig. 9(c) shows a magnified part of the three dimensional surface profile obtained by using the PRDS method, the periodical microlens array can be clearly seen. The cross section profile along a line passing through the centers of microlens array is shown in Fig. 9(f). The convergence time for obtaining this result was about five minutes. Results using the PRSS method (Fig. 9d and g) were obtained after about nine minutes. A comparison with the measurement done by a Zygo Newview white light interferometer (WLI) (Fig. 9e and h), demonstrate the efficiency of the proposed method. The SSE of the results obtained by the PRDS method is about 50% better compared with the PRSS measurements.

4. Conclusions

A technique for the measurement of the shape using double sequences diffraction patterns recorded at multiple illumination

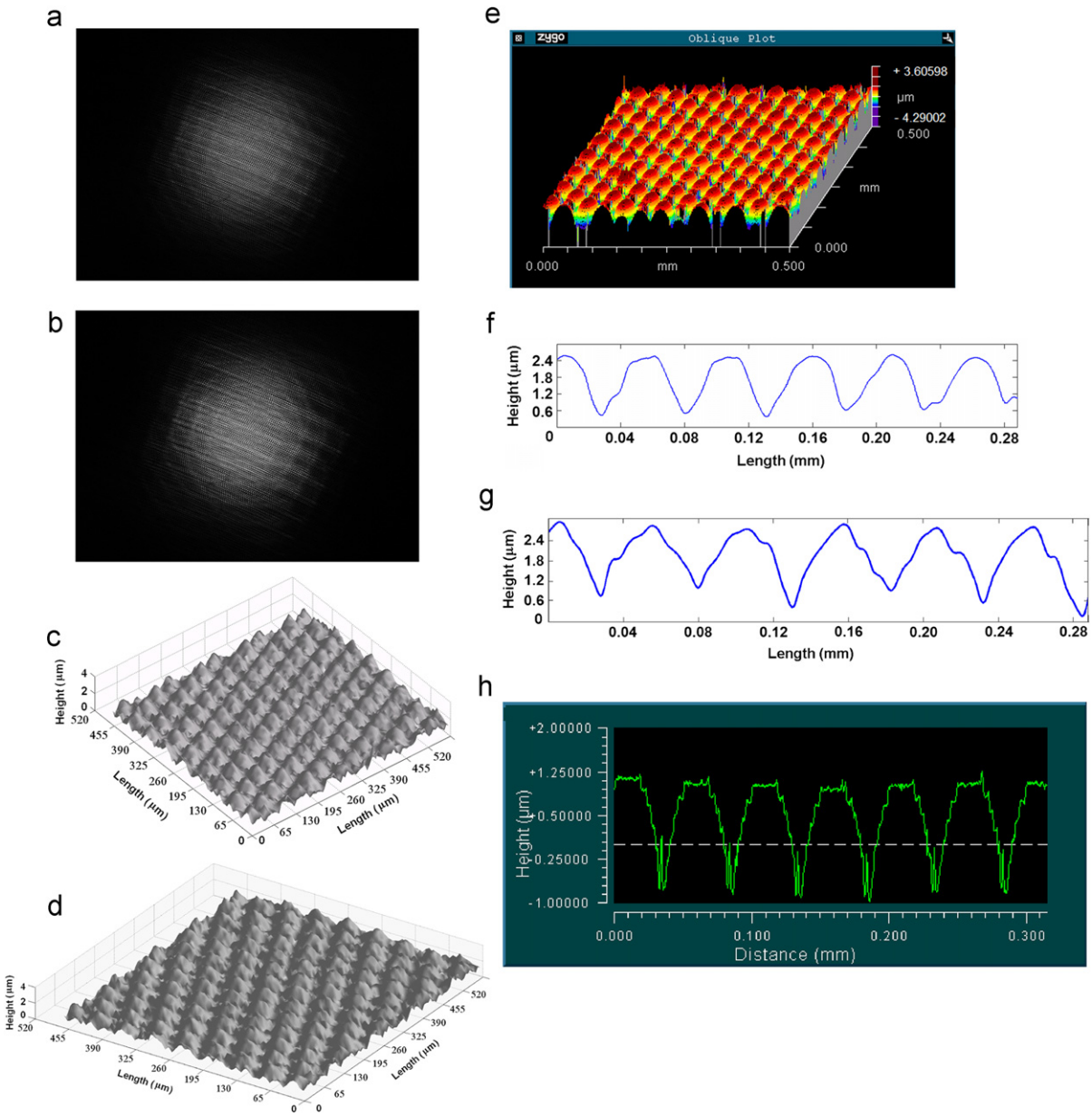

Fig. 9. Experimental results: CCD captured images at (a) 750 nm and (b) 850 nm, 3D surface obtained by (c) PRDS, (d) PRSS and (e) WLI; cross section profile obtained by (f) PRDS, (g) PRSS and (h) WLI.

wavelengths was demonstrated by both simulation and experimental results. The improvements of the PRDS compared with the PRSS were theoretically analyzed and discussed. Comparisons showed that the advantages of the PRDS are faster convergence speed and more accurate results. The PRDS technique is more suitable than the PRSS when the object surface height is several times larger than the illumination wavelengths. The performances of the PRDS technique have been systematically demonstrated by simulation under different conditions and in an experiment where the optical surface profile of a microlens array was measured. The proposed technique can be used to characterize different kind of micro-structures.

Acknowledgment

Peng Bao acknowledges the financial support of the China Scholarship Council (CSC).

Reference

[1] D. Malacara, Optical Shop Testing, John Wiley & Sons Inc, 1992.
[2] F. Chen, G.M. Brown, M. Song, Optical Engineering 39 (2000) 10.
[3] P.S. Huang, Q. Hu, F. Jin, F. Chiang, Optical Engineering 38 (1999) 1065.
[4] C. Quan, X.Y. He, C.F. Wang, C.J. Tay, H.M. Shang, Optics Communications 189 (2001) 1.
[5] B.L. Danielson, C.Y. Boisrobert, Applied Optics 30 (1991) 21.
[6] Y.J. Rao, D.A. Jackson, Measurement Science and Technology 7 (1996) 981.
[7] I. Yamaguchi, A. Yamamoto, S. Kuwamura, Applied Optics 37 (1998) 28.
[8] U. Schnars, W. Jüptner, Measurement Science and Technology 13 (2002) R85.
[9] U. Schnars, W. Jüptner, Digital holography: digital hologram recording, numerical reconstruction, and related techniques, Springer, 2005.
[10] I. Yamaguchi, T. Zhang, Optics Letters 22 (1997) 16.
[11] I. Yamaguchi, T. Matsumura, J. Kato, Optics Letters 27 (2002) 13.
[12] W. Osten, T. Baumbach, W. Jüptner, Optics Letters 27 (2002) 20.
[13] T. Baumbach, W. Osten, C. Kopylow, W. Jüptner, Applied Optics 45 (2006) 5.
[14] R.W. Gerchberg, W.O. Saxton, Optik 35 (1972) 237.
[15] B. Gu, G. Yang, Acta Optica Sinica 1 (1981) 517.
[16] J.R. Fienup, Optics Letters 3 (1978) 27.
[17] C. Kohler, F. Zhang, W. Osten, Applied Optics 48 (2009) 4003.
[18] H.M.L. Faulkner, J.M. Rodenburg, Physical Review Letters 93 (2004) 023903.

[19] G. Pedrini, W. Osten, Y. Zhang, Optics Letters 30 (2005) 833.
[20] P. Almoro, G. Pedrini, W. Osten, Applied Optics 45 (2006) 8596.
[21] F. Zhang, G. Pedrini, W. Osten, Physical Review A 75 (2007) 043805.
[22] P. Almoro, J. Glückstad, S.G. Hanson, Optics Express 18 (2010) 18.
[23] A. Jesacher, W. Harm, S. Bernet, M. Ritsch-Marte, Optics Express 20 (2012) 5.
[24] P. Bao, F. Zhang, G. Pedrini, W. Osten, Optics Letters 33 (2008) 4.
[25] P. Bao, F. Zhang, G. Pedrini, W. Osten, Proceedings of the SPIE 6995 (2008).
[26] J.N. Cederquist, C.C. Wackerman, Journal of the Optical Society of America A 4 (1987) 9.
[27] J.W. Goodman, Introduction to Fourier Optics, McGraw-Hill, 1996.
[28] 〈http://www.schott.com/advanced_optics/chinese/our_products/materials/data_tools/index.html?so=china&lang=english〉, Schott AG, 2011.